Modelling of a Deployable Ring Antenna Truss Structure using a Central Difference Scheme

Rebecca Durrant
College of Engineering
Swansea University
Swansea UK
916039@swansea.ac.uk

***Abstract* - This paper describes an investigation into the geometrical design, dynamic analysis, and deployment methods of a double-ring, deployable antenna truss structure. A deployable structure would give satellites more flexibility in communication. A central difference scheme was compared to the exact solution of a single degree of freedom system and subsequently used to approximate a multiple degrees of freedom dynamic response. Two deployment methods were considered, a free expansion of a preloaded structure, and applying a force to a rope along the outer ring of the structure. Analysis showed that aiding deployment with an applied force gives a shorter deployment time.**

Keywords - Central difference scheme, deployable antenna, dynamic analysis, truss structure.

I. INTRODUCTION

As modern spacecraft are beginning to operate further away from the earth, it is an advantage to have larger antennae with higher transmission power to reduce attenuation effects on communication with mission control centres based on earth. However, fixed antenna structures have volume and mass constraints dependent on the size of the payload bay and the rocket dimensions and capabilities. These constraints limit the effective area, range, and gain of the antenna.

A. Motivation

Deployable antennae structures are becoming increasingly useful to give spacecraft additional flexibility in communications by allowing larger or more antennas to be used on a satellite for relatively little extra cost.

Using deployable antennae structures will also decrease the volume the antennae will take up in the payload, increasing the payload area available to carry additional payloads or decreasing the total mass of the payload. This makes it possible to reduce launch costs, or to decrease the price per kilogram launched. Deployable truss structures have a reduced mass compared to large, fixed antenna structures, which further reduces total payload mass and therefore launch costs.

Deployable double-ring structures also have other applications within the space industry. These structures would also be suitable for use in a solar array, as a reflector to concentrate sunlight to an existing solar array, or to replace existing large, external, fixed ring structures on satellites or spacecraft. For example, to replace a damaged antenna or solar array on the International Space Station.

A single-ring deployable structure has previously been suggested for use in space as a deployable antenna structure [1-3], and also for other structural purposes [5]. However, the stiffness of a large diameter single-ring truss structure is low [5]. For this reason, a double-ring deployable truss structure should be investigated to increase the stiffness.

B. Objective

The aim of this project is to carry out further investigation of the explicit dynamics of a double-ring deployable antenna truss structure through MATLAB [6] analysis.

Using a double-ring structure will increase the overall mass and volume compared to a single ring structure but will also increase the stiffness as required for large-calibre antennae. The increased mass and volume of a double-truss structure is still lower than that of a fixed structure, and allows for a larger aperture [7].

Several different types of double-ring structures have been previously proposed [8-12].

Previous studies have investigated the statics [13], dynamics [5], deployment mechanisms [5], cable tensioning [9, 14], and structural optimisation [5] of double-ring truss structures.

C. Methodology

The analysis will utilise a central difference scheme to estimate the dynamic response of a truss structure. A central difference scheme is a type of finite difference method used to approximate differential equations. A central difference scheme approximates differential equations with linear equations by using previous variables [15]. The linear equations can then be solved explicitly, to give an explicit solution. In this project, the central difference scheme uses a forward difference to approximate the dynamic response of a structure by using the structural coordinates at previous time steps.

The rest of this paper will consist of six sections. Section II describes the 3D model of the structure, including the joints and truss types. It also describes the geometry of the proposed structure, using the relations between the number of sections in the structure, the height of the vertical members, and the radius of the

outer ring to define the coordinates of the nodes of the structure. Finally, this section explains the force calculation.

Section III will explore methodology, explaining the central difference scheme and applying it to a single truss. Section IV will explain the simulation of the deployment, including two deployment methods. Section V will state the results of both deployment methods. Finally, Section VI will conclude the paper, stating achievements, discussing the results and noting potential future work.

II. 3D Model

A double-ring truss structure has an inner and an outer ring. The structure consists of multiple sections, such as those shown in Figure 01.

A. *Pin-joint trusses & Ropes*

The truss structure will consist of a frame of stiff vertical and horizontal trusses of fixed lengths, and of diagonal elastic members of variable lengths. The fixed length trusses were assigned truss types of 1 to 4. The variable lengths represent elastic members that will undergo different stresses and strains during the undeployed state, deployment, and the final deployed state. The elastic members were assigned truss types 5 to 9. In Figure 01 truss types 1 to 4 are shown in black, and types 5 to 9 are shown in colour.

There are two types of hinge, a six-truss and a seven-truss hinge. Each of the trusses connects via pin joint to one of these hinges at each end.

B. *Geometric Constraints*

To ensure that deployment is possible with this assortment of fixed and variable lengths, there must be geometrical constraints on the structure. For this reason, the structural relations used to define the geometry of the structure in this analysis were the same geometric relations as previously described by Dai et al [5].

The number of sections in the structure is N. The outer radius, R, height, H, and N are chosen parameters. The section angle, α, is calculated from the number of sections as shown in (1).

$$\alpha = \frac{2\pi}{N} \tag{1}$$

The outer section length, D, was derived using trigonometry to give (2).

$$D = 2\,R \sin\left(\frac{\alpha}{2}\right) \tag{2}$$

The inner radius, r, was also derived using trigonometry as shown in (3).

$$r = R\frac{1 - \sin\left(\frac{\alpha}{2}\right)}{1 + \sin\left(\frac{\alpha}{2}\right)} \tag{3}$$

The inner section length was derived from the inner radius in (4).

$$d = 2\,r \sin\left(\frac{\alpha}{2}\right) \tag{4}$$

All dimensions are shown in Figure 2 & 3. The heights of both the inner ring and the outer ring must be equal to allow deployment and folding [5].

The geometry description given here is for a fully deployed structure where N = 6, H = 2 m, and R = 10 m, with corresponding nodes as shown in Figure 01.

Figure 03 shows the nodes in one section of the six section structure. The coordinates of node 1 (N1) are (R,0,0). The coordinates of N13 are (r,0,0). The z-coordinates N7 and N19 can be calculated by adding H to the coordinates of N1 and N13 respectively.

The x-coordinate of N2 can be calculated by multiplying R by cosine(α). All lower nodes on the outer ring (N1 to N6) can be calculated using (5), where N is the section number.

$$x = R\cos(\alpha(N-1)) \tag{5}$$

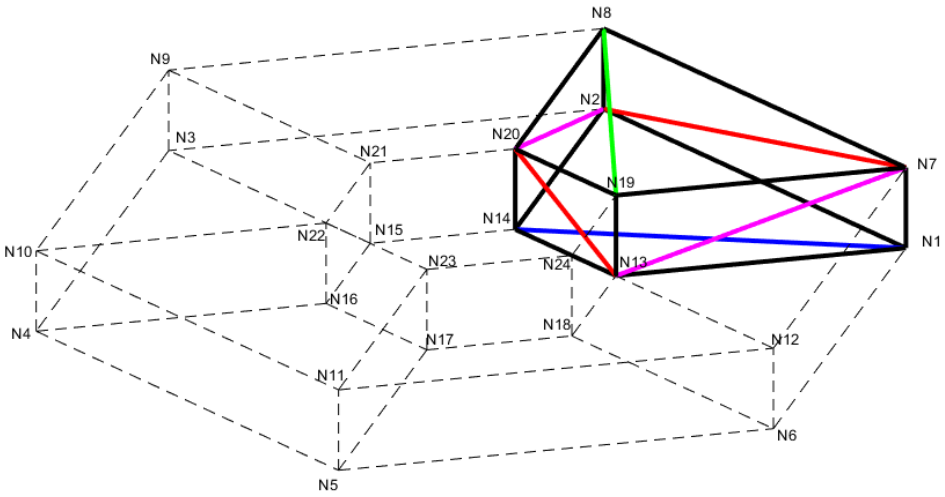

FIGURE 01
LABELLED NODE DIAGRAM OF THE FULLY DEPLOYED STRUCTURE SHOWING ONE SECTION

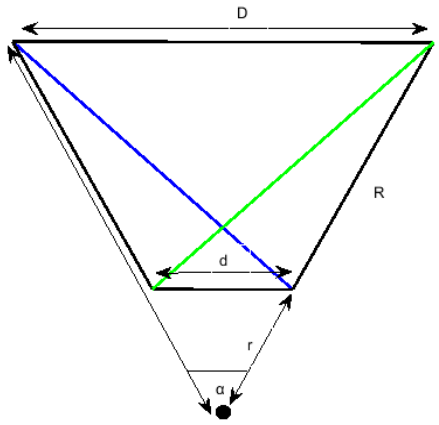

FIGURE 02
DIMENSIONED DIAGRAM OF PLAN VIEW OF ONE SECTION OF THE STRUCTURE

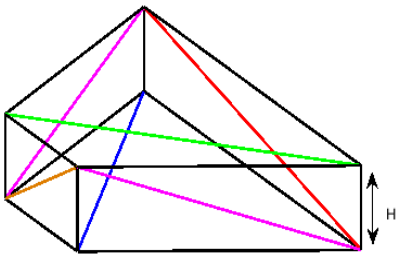

FIGURE 03
ONE SECTION OF A DOUBLE-RING TRUSS STRUCTURE, PARTIALLY DIMENSIONED

The x-coordinates of N14 to N18 can be calculated in a similar method using the inner radius, *r*, as shown in (6).

$$x = r\cos(\alpha(N-1)) \tag{6}$$

The y-coordinates of N2 and N14 are calculated similarly, using sine(α) instead of cosine(α). This is shown in (7) for the outer.

$$y = R\sin(\alpha(N-1)) \tag{7}$$

The y-coordinates of the inner ring were again calculated similarly using *r*, as shown in (8).

$$y = r\sin(\alpha(N-1)) \tag{8}$$

The z-coordinates of all the lower nodes on both the outer and inner ring are zero, including N2 and N14.

The x- and y-coordinates of N8 and N20 are equal to those of N2 and N14 respectively. The z-coordinates are equal to *H*. The diagonal trusses seen in Figure 03 are each defined as a different truss type. They are all of variable length, meaning that the length of each type varies as the structure deploys. Each diagonal alternates orientation for each section. For example, the green diagonal truss between N19 and N8 would continue from N8 to N21, and from N21 to N10 and so on, as seen in Figure 04.

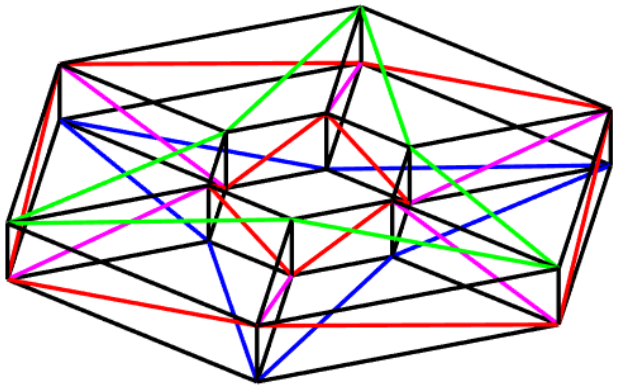

FIGURE 04
FULL DIAGRAM OF THE FULLY DEPLOYED STRUCTURE WITH SIX SECTIONS, SHOWING STIFF TRUSSES IN BLACK AND ELASTIC MEMBERS IN COLOUR

For the undeployed structure, the outer radius is known as *R'*, and the inner radius as *r'*. An example of the undeployed structure in Figure 04 folded to an *R'* of 5 m is shown in Figure 05. The undeployed structure also introduces the angle θ, which is described by (9) [13].

$$\theta = \arccos\left(\frac{R'}{R}\right) \tag{9}$$

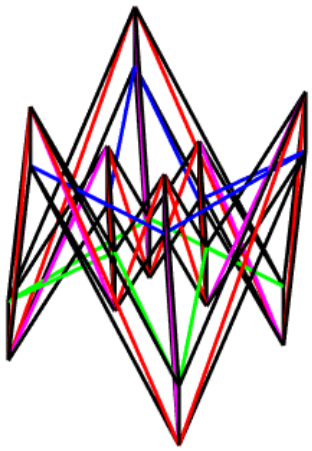

FIGURE 05
DIAGRAM OF THE PARTIALLY FOLDED STRUCTURE

The following geometry description is of an undeployed structure with a deployment angle of θ and the rest of the parameters are the same as the previously used example, where $N = 6$, $H = 2$ m, and $R = 10$ m.

The x-coordinates of the outer ring are calculated using the previous method for the fully deployed structure, using *R'* in place of *R* as shown in (10).

$$x = R'\cos(\alpha(N-1)) \tag{10}$$

The x-coordinates of the inner ring are calculated using *r'* rather than *R'*, as shown in (11).

$$x = r'\cos(\alpha(N-1)) \tag{11}$$

Likewise, the y-coordinates of the outer ring are calculated with (12).

$$y = R' \sin(\alpha(N-1)) \tag{12}$$

The y-coordinates of the inner ring are calculated with (13).

$$y = r' \sin(\alpha(N-1)) \tag{13}$$

The z-coordinate of N1 is 0. The z-coordinate of N2 can be calculated as in (14). The z-coordinates of the lower outer ring nodes alternate between zero and (14). The undeployed structure, this time with an *R'* of 8 m for clarity, can be seen with labelled nodes in Figure 06.

$$z = D \sin(\theta) \tag{14}$$

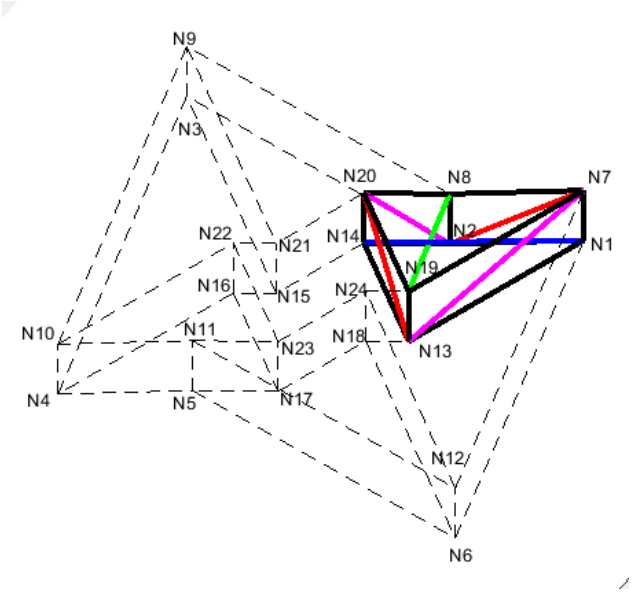

FIGURE 06
NODE LABELLED DIAGRAM OF THE PARTIALLY FOLDED STRUCTURE

The z-coordinates of N7 and N8 are again calculated by adding *H* to the z-coordinates of N1 and N2 respectively.

The z-coordinate of N13 is calculated using (15).

$$z = (R-r)\sin(\theta) \tag{15}$$

The z-coordinate of N14 is calculated with (16).

$$z = (R-r)\sin(\theta) - d\sin(\theta) \tag{16}$$

The z-coordinates of N19 and N20 are calculated by adding *H* to the z-coordinates of N13 and N14 respectively.

C. Logarithmic Force

The force in each truss was calculated using a logarithmic method as opposed to using the linear Hooke's Law method. This is because Hooke's Law allows for a negative truss length, whereas the logarithmic method has asymptotes at strains of -100 % and 100 %. The accuracy of Hooke's Law is limited to small strains below the Young's Modulus of the material [16], and the logarithmic approximation is more accurate for larger strains, dependent on materials. The strains of this model remained below 37 %, so it was not necessary to use alternative methods such as neo-Hooke which would more accurate for the much larger deformations of hyper elastic materials.

The logarithmic equation use to calculate force used is shown in (17).

$$F = EA \ln\frac{L}{L_0} \tag{17}$$

III. METHODOLOGY

A model of the structure was programmed in MATLAB as a sub-function of the main code, taking inputs of *N*, *H*, *R*, and *R'* to give outputs of the coordinate matrix, *X*, the connectivity matrix, *iX*, and the initial lengths of each truss type in the fully deployed structure, L_0. Pseudo code of the coordinate matrix construction within the structure function can be seen in Figure 07, using the previously stated coordinate calculations.

```
Structure Function

INPUTS: N, H, R, R'
OUTPUT: X                                   (Coordinate matrix)

DEFINE: α = 2π/N                            (Section angle, radians)
DEFINE: D = 2Rsin(α/2)                      (Outer ring horizontal length, m)
DEFINE: r = R(1-sin(α/2))/(1+(α/2))         (Inner radius, m)
DEFINE: d = 2rsin(α/2)                      (Inner ring horizontal length, m)

DEFINE: r'= R'(1-sin(α/2))/(1+(α/2))        (Inner radius, undeployed, m)
DEFINE: θ = arccos(R'/R)                    (Deployment angle, radians)

FOR number of sections

     CALCULATE x coordinates of nodes
     CALCULATE y coordinates of nodes
     CALCULATE z coordinates of nodes

     IF node number is odd

          CALCULATE z coordinates for every other node in the rings

     ELSEIF node number is even

          CALCULATE z coordinates for remaining nodes

     END IF

END FOR

STORE coordinates in a matrix
```

FIGURE 07
PSEUDO CODE OF THE COORDINATE MATRIX CONSTRUCTION

Pseudo code describing the construction of the connectivity matrix within the structure function and explaining the different truss types is shown in Figure 08.

```
Structure Function

INPUTS: N, H, R, R'
OUTPUT: iX (connectivity matrix)

FOR number of sections

     DEFINE: node connectivity for type 1 trusses (Horizontal outer ring members)
     DEFINE: node connectivity for type 2 trusses (Horizontal inner ring members)
     DEFINE: node connectivity for type 3 trusses (Vertical members)
     DEFINE: node connectivity for type 4 trusses (Horizontal members)
     DEFINE: node connectivity for type 5 trusses (Outer diagonal members)
     DEFINE: node connectivity for type 6 trusses (Inside diagonal members)
     DEFINE: node connectivity for type 7 trusses (Vertical diagonals between rings)
     DEFINE: node connectivity for type 8 trusses (Upper horizontal diagonals)
     DEFINE: node connectivity for type 9 trusses (Lower horizontal diagonals)

END FOR

STORE node connections as connectivity matrix
```

FIGURE 08
PSEUDO CODE OF THE CONNECTIVITY MATRIX CONSTRUCTION

Pseudo code of the length calculation also within the structure function is shown in Figure 09.

```
Structure Function

INPUTS: N, H, R, R'
OUTPUT: L0          (Length matrix)

   FOR length of connectivity matrix

      GET coordinates of first node
      GET coordinates of second node
      CALCULATE length between nodes
      STORE length in Length matrix

   END FOR
```

FIGURE 09
PSEUDO CODE OF LENGTH CALCULATION

A. *Central Difference Scheme*

To validate the accuracy of the central difference scheme, it was tested alongside the exact solution for a single degree of freedom system with no applied force.

Equation (18) estimates the velocity at time *n* by taking the difference in displacement at the subsequent and previous time steps, and dividing by double the time step.

$$\dot{x}_n = \frac{x_{n+1} - x_{n-1}}{2\,\Delta t} \tag{18}$$

Equation (19) calculates acceleration at time *n*.

$$\ddot{x}_n = \frac{x_{n+1} - 2x_n + x_{n-1}}{\Delta t^2} \tag{19}$$

Equation (20) is the equation of motion for a system with mass, stiffness and damping [17].

$$M\ddot{x} + c\dot{x} + kx = 0 \tag{20}$$

To derive the equations used for the central difference scheme, equations for velocity (18) and acceleration (19) were substituted into the equation of motion (20). This was rearranged to give (21). The displacement at time *n* is given by x_n, Δt is the time step, *K* is the stiffness, and *M* is the mass.

$$x_{n+1} = \frac{C\,\Delta t\,x_{n-1} + 2\,M\,(2x_n - x_{n-1}) - 2\,\Delta t^2 K x_n}{2\,M + C\,\Delta t} \tag{21}$$

Initially, zero damping was applied to reduce complexity of comparing the central difference scheme to the exact solution. The simplified equation for displacement is shown in (22).

$$x_{n+1} = 2x_n - x_{n-1} - \frac{Kx_n\Delta t^2}{M} \tag{22}$$

The exact solution was calculated with (23) [17], where ζ is the damping ratio, ω_n is the natural frequency of the system, *t* is the time, V_0 is the initial velocity, and x_0 is the initial displacement.

$$x_{n+1} = e^{-\zeta\omega_n t}\left(\frac{V_0}{\omega_n}\sin(\omega_n t) + x_0\cos(\omega_n t)\right) \tag{23}$$

Without damping, this equation was simplified to (24) [17], where all constants are as previously defined.

$$x_{n+1} = \frac{V_0}{\omega_n}\sin(\omega_n t) + x_0\cos(\omega_n t) \tag{24}$$

The system was given a mass of 1 kg and a stiffness of 1 N/m. The time step, Δt, was decreased from 1 second to find a suitable accuracy for use on the full model whilst also being able to run the program in a reasonable amount of time. Figure 10 compares the central difference scheme to the exact solution for a time step of one second. This gives very poor results and could not be used. Figure 11 uses a time step of 0.1 second. This was considerably more accurate than a time step of one second, but not accurate enough to use in a full dynamic analysis. Figure 12 and 13 show time steps of 0.01 second and 0.001 second respectively.

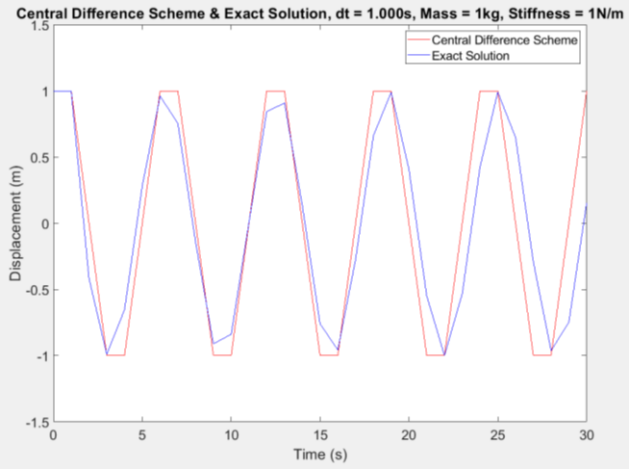

FIGURE 10
DISPLACEMENT AGAINST TIME FOR A TIME STEP OF ONE SECOND

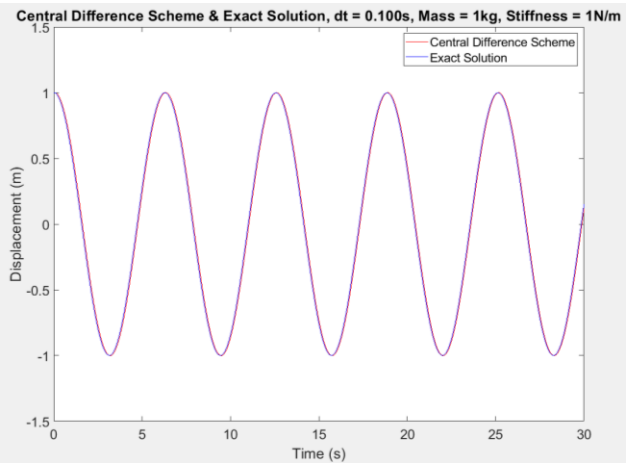

FIGURE 11
DISPLACEMENT AGAINST TIME FOR A TIME STEP OF 0.1 SECOND

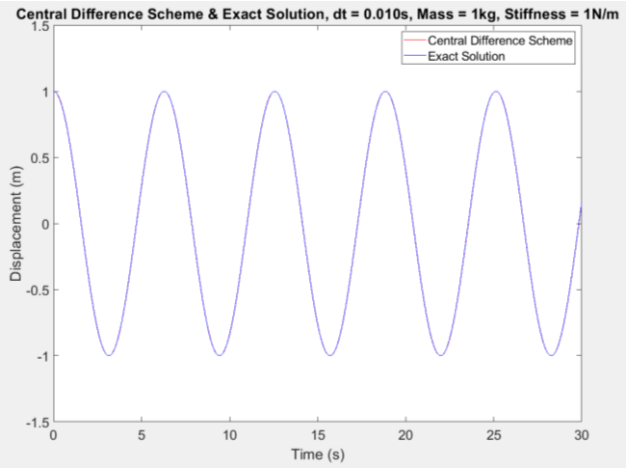

FIGURE 12
DISPLACEMENT AGAINST TIME FOR A TIME STEP OF 0.01 SECOND

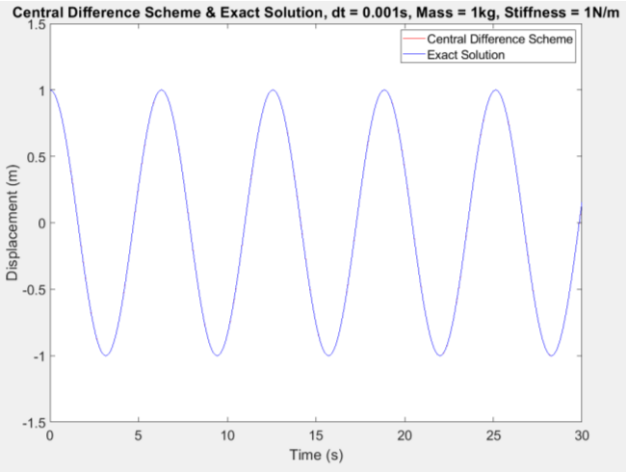

FIGURE 13
DISPLACEMENT AGAINST TIME FOR A TIME STEP OF 0.001 SECOND

The error between the two solutions was calculated as shown in the pseudo code in Figure 14.

A time step of 1 second gave an error of ± 2.00 mm. This time step had a computation time of 1.024 seconds.

The time step of 0.1 second gave an error of ± 0.05 mm with a computation time of 1.142 seconds.

The time step of 0.01 second gave an error of ± 0.05 mm with a computation time of 1.184 seconds.

The time step of 0.001 second gave an error of 0.00 mm with a computation time of 1.291 seconds.

```
Error Calculation in Single Degree of Freedom System

CALCULATE difference between explicit and exact solutions
CALCULATE maximum difference
ROUND maximum difference to 1mm
PRINT maximum difference to 1mm
```

FIGURE 14
PSEUDO CODE OF THE ERROR CALCULATION

Only the time step of 0.001 second was accurate to 0.00 mm. Both 0.1 and 0.01 second time steps were accurate to ± 0.05 mm.

The time step of 0.001 second had an increase of computation time of 9.1 % from the previous time step of 0.01 second, whereas a time step of 0.01 second had only a 3.6 % increase in computation time when compared to the time step of 0.1 second.

As the tested structure had an outer radius of 10 m, an error of ± 0.05 mm was considered acceptable [18], meaning these three time steps were sufficiently accurate to use on the full model, but a time step of 0.01 second was chosen as the computation time of the full model took far longer than a single degree of freedom system.

With a time step of 0.01 second, the compute time for the full structure deployment was around 110 seconds. This increased to around 1420 seconds with a time step of 0.001 second.

There were also limitations in memory storage in MATLAB when using the time step of 0.001 second for large structures.

B. Single Truss Problem

Once the central difference scheme was tested and validated, it was applied to a single truss structure with multiple degrees of freedom. The truss only moved in the x-direction. This allowed testing of the central difference scheme on a small multiple degree of freedom structure for simpler analysis.

To account for damping in the single truss analysis the stiffness term, Kx_n, in (21) was replaced by F_x, the resultant force in the truss member in the x-direction. This is shown in (25). This force was calculated in each iteration by the tension or compression of the truss, as in (17).

$$x_{n+1} = \frac{C\,\Delta t\,x_{n-1} + 2\,M\,(2x_n - x_{n-1}) - 2\,\Delta t^2\,F_x}{2\,M + C\,\Delta t} \quad (25)$$

The parameters used for the single truss analysis are as follows: a truss mass of 1 kg, an initial length of 1 m, a Young's Modulus of 10 Pa, and a time step of 0.1 second.

A graph of showing the displacement of one node against time using the central difference scheme without damping is seen in Figure 15.

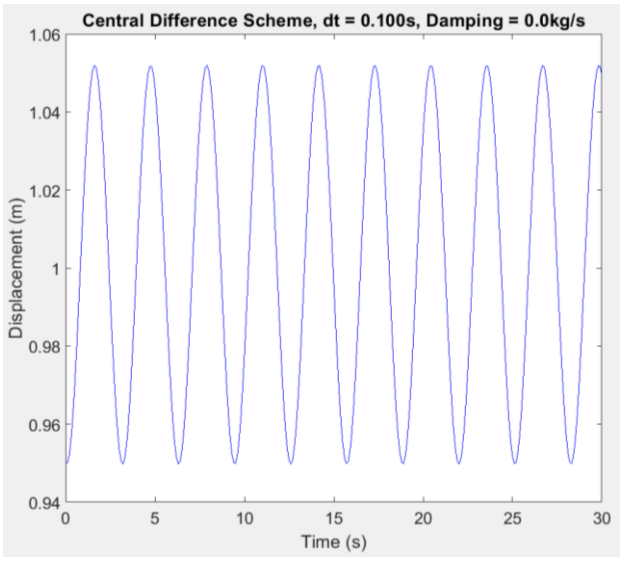

FIGURE 15
DISPLACEMENT IN THE X-DIRECTION OF ONE NODE OF AN UNDAMPED SINGLE TRUSS STRUCTURE

Figure 16 shows the same scheme using a damping constant of 0.5 kg/s.

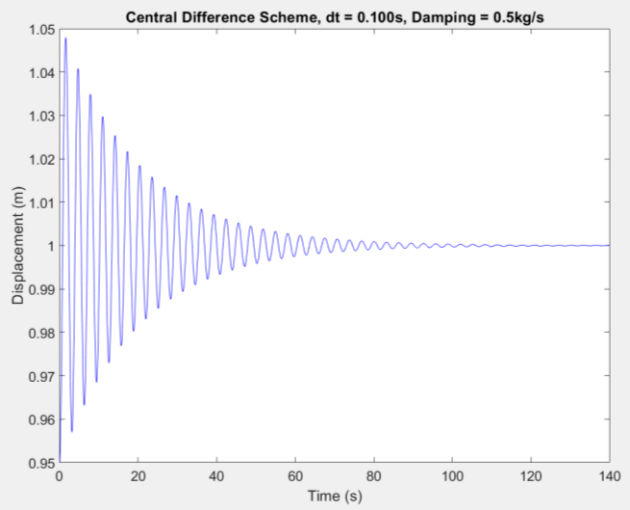

FIGURE 16
DISPLACEMENT IN THE X-DIRECTION OF ONE NODE OF A DAMPED SINGLE TRUSS STRUCTURE

Figure 15 proves that the structure without damping will never converge to its desired position. Figure 16 shows that with a damping of 0.5 kg/s, the truss takes approximately 139 seconds to reach its final structure to within 1 mm.

This testing of a single truss proves that using a central difference scheme, a damped, folded truss structure can deploy fully after some oscillation. In the full double-ring structure, the damping should be optimised to minimise oscillation.

IV. SIMULATION OF ANTENNA DEPLOYMENT

The central difference scheme in (25) was applied to the x-, y-, and z-coordinates of each node in the structure in the initial configuration similar to Figure 05 with an *R'* of 0.6m. Here, *M* represents a diagonal matrix of the masses of each node in the structure. The force, *F*, was calculated for each truss by (17) and applied cumulatively to each node. The force changed with each time step as the length of the truss changed.

All of the vertical and horizontal members shown in black in the structure (Figure 04) are of a fixed length. For the purpose of this analysis, these trusses were given a Young's Modulus of 100 Pa, a cross-sectional area of 1 m^2, and a mass of 1 kg. The rest of the members are elastic and were modelled with a Young's Modulus of 10 Pa, a cross-sectional area of 1 m^2, and a mass of 1 kg.

Specific material data was not considered to be important in this model. The trusses in a physical model would be designed so as to withstand the maximum stresses and strains calculated, rather than calculating the forces in a truss with given properties. It was important to give the trusses of fixed length a higher stiffness than the elastic members to ensure proper deployment.

There were also software limitations preventing the use of large Young's Modulus's in conjunction with small cross-sectional areas.

A. *Elastic Deployment*

Truss types 1 to 4 were stiff trusses of a constant length. This included all vertical and horizontal members.

Truss types 5 to 9 were considered to be elastic and of variable length depending on the deployment angle.

The undeployed, preloaded structure has stresses in the trusses that would allow self-deployment once the antenna structure was released into an open area, such as space.

Various amounts of damping were applied to the system, from 0.4 kg/s to 1.2 kg/s with 0.1 kg/s increments.

The truss structure used in this analysis had 8 sections, a height of 2 m, a deployed outer radius of 10 m, and an initial outer radius of 0.6 m.

Pseudo code of the construction of the mass matrix and force calculations is shown in Figure 17 and Figure 18 respectively.

```
Mass Vector function                    (Constructs a mass matrix)

Inputs: X, iX, mass                     (Takes vector of masses of truss types)
Output: M                               (Returns a matrix of masses at nodes)

FOR length of connectivity matrix

     STORE masses of each truss in a matrix

END FOR


for length of connectivity matrix

     GET first node number of truss
     GET second node number of truss

     STORE half of the truss mass to each node cumulatively
     STORE node masses in a mass matrix

END FOR
```

FIGURE 17
PSEUDO CODE OF CONSTRUCTION OF THE MASS MATRIX CONSTRUCTION

```
Force Calculations

FOR number of time steps

     FOR length of connectivity matrix

          GET first node of truss
          GET second node of truss
          GET truss type

          CALCULATE difference in x coordinates between two nodes
          CALCULATE difference in y coordinates between two nodes
          CALCULATE difference in z coordinates between two nodes

          CALCULATE length of truss from coordinates
          CALCULATE force from new length

          ASSIGN force to x direction
          ASSIGN force to y direction
          ASSIGN force to z direction

          ASSIGN directional force to nodes

     END FOR

END FOR
```

FIGURE 18
PSEUDO CODE OF FORCE CALCULATIONS FOR ELASTIC DEPLOYMENT

B. *Applied Force Deployment*

A secondary analysis was also carried out, where the red diagonal on the outer ring from N7 to N2 shown in Figure 03 is a singular rope running around the whole outer ring with a constant applied force. This rope is defined as truss type 5. The rope passes through a frictionless roller inside each hinge.

The rest of the structural configuration was the same as the previous analysis, with eight sections, a height of

2 m, a deployed outer radius of 10 m, and an initial outer radius of 0.6 m.

This structure also contains stresses in its undeployed state which would allow the structure to self-deploy given an open area, along with the additional force applied to the type 5 rope to aid the deployment of the antenna structure to its fully unfolded configuration.

Damping of 0.7 kg/s was applied to the system. This value was chosen as a medium value from previous tests.

The red diagonal on the inner ring from N13 to N20 is also a rope with no applied force. As such it experiences no compressive force, so where the resulting force from (17) would be negative due to L being shorter than L_0, the force is set to zero. This diagonal is defined as truss type 6. The other diagonal trusses are all of an elastic nature, also assumed to experience tension only, as calculated by (17).

The applied force in conjunction with the changes to the truss types in this secondary analysis will reduce oscillation of the structure after it deploys to its full size compared to the elastic analysis.

The changes to the method of calculation of the forces on each truss type can be seen in the pseudo code shown in Figure 19. The tension and compression forces where required were calculated with (17).

```
Force Calculations

FOR number of time steps

    FOR length of connectivity matrix

        GET first node of truss
        GET second node of truss
        GET truss type

        CALCULATE difference in x coordinates between two nodes
        CALCULATE difference in y coordinates between two nodes
        CALCULATE difference in z coordinates between two nodes

        CALCULATE length of truss from coordinates

        IF truss type is 5

            DEFINE applied force

        ELSEIF truss type is more than 5

            IF truss is under compression

                SET force to zero

            ELSE
                CALCULATE force

            END IF

        ELSE

            CALCULATE force

        END IF

    END FOR

END FOR
```

FIGURE 19
PSEUDO CODE OF FORCE CALCULATIONS FOR APPLIED FORCE DEPLOYMENT.

Due to the applied force, energy is required for this method of deployment. The energy used to pull the rope is calculated by multiplying the applied force, F, by the length of rope that is pulled during deployment, L. This is shown in (26).

$$E = F\,L \tag{26}$$

The length of rope pulled is calculated by the difference in the initial length of the rope around the whole outer ring and the final length of the same rope in the fully deployed structure. This length is constant for a given initial and final radius.

V. RESULTS

A. Elastic Deployment

The deployment times for various amounts of damping is shown in Table I. The maximum strain for all amounts of damping was 36.76 %. This was the initial deformation of the elastic truss type 6 before deployment.

TABLE I
STRUCTURE DEPLOYMENT TIME COMPARED TO DAMPING

Time Step (s)	Damping (kg/s)	Deploy Time (s)	Maximum Stress (Pa)
0.01	0.4	147.62	33.26
0.01	0.5	132.04	31.86
0.01	0.6	112.63	30.46
0.01	0.7	97.91	29.09
0.01	0.8	86.05	27.78
0.01	0.9	85.01	26.52
0.01	1.0	89.29	25.32
0.01	1.1	97.05	24.19
0.01	1.2	132.55	23.13

The stresses in the initial configuration of the antenna structure were in the range -12.49 Pa to 3.13 Pa for the diagonal members. The fixed length trusses had an initial stress of zero. A damping of 0.9 kg/s gave the shortest deployment time and was therefore used for further analysis of the maximum stresses and strains in each truss type, shown in Table II and Table III respectively.

TABLE II
MAXIMUM STRESS IN EACH TRUSS TYPE

Type	L_0 (m)	E (Pa)	A (m^2)	Max. Force (N)	Max. Stress (Pa)
1	7.65	100	1.00	6.69	6.69
2	3.42	100	1.00	5.48	5.48
3	2.00	100	1.00	26.52	26.52
4	5.54	100	1.00	14.13	14.13
5	7.91	10	1.00	2.35	2.35
6	3.96	10	1.00	3.13	3.13
7	5.89	10	1.00	2.57	2.57
8	7.54	10	1.00	0.26	0.26
9	7.54	10	1.00	0.26	0.26

The maximum truss lengths and maximum strain during the first analysis for each truss type is defined in Table III. The first four truss types were intended to be rigid, and this was to be achieved by using a higher Young's Modulus for these truss types. As the material data is not realistic, the lengths of these trusses did vary.

TABLE III
MAXIMUM STRAIN IN EACH TRUSS TYPE

Type	L_0 (m)	Maximum Length (m)	Max. Strain (%)
1	7.65	8.18	6.92
2	3.42	3.61	5.63
3	2.00	2.61	30.37
4	5.54	6.97	25.96
5	7.91	10.01	26.54
6	3.96	5.41	36.76
7	5.89	7.61	29.25
8	7.54	7.73	2.60
9	7.54	7.73	2.60

B. *Applied Force Deployment*

Forces between 0.01 N to 0.05 N were applied to the rope at 0.005 N increments to force the deployment of the structure.

The maximum strain for all tests was again 36.76 % during the initial configuration. The maximum stress in the structure was 19.78 Pa in truss type 3 in the initial configuration. The deployment times for different applied forces is shown in Table IV.

TABLE IV
STRUCTURE DEPLOYMENT TIME, APPLIED FORCE, AND ENERGY REQUIREMENT

Time Step (s)	Applied Force (N)	Deploy Time (s)	Energy Required (J)
0.01	0.010	46.40	0.14
0.01	0.015	42.07	0.21
0.01	0.020	37.97	0.28
0.01	0.025	36.64	0.35
0.01	0.030	36.58	0.42
0.01	0.035	37.16	0.49
0.01	0.040	37.99	0.56
0.01	0.045	38.01	0.63
0.01	0.050	38.12	0.70

The minimum deployment time occurred with an applied force of 0.03N, therefore this force was used to investigate the stress and strain effects each different truss type.

The maximum stresses produced in the trusses during the deployment are shown in Table V.

TABLE V
MAXIMUM STRESS IN EACH TRUSS TYPE

Type	L_0 (m)	E (Pa)	A (m^2)	Max. F (N)	Max Stress (Pa)
1	7.65	100	1.00	8.09	8.09
2	3.42	100	1.00	4.46	4.46
3	2.00	100	1.00	19.78	19.78
4	5.54	100	1.00	18.49	18.49
5	7.91	10	1.00	0.03	0.03
6	3.96	10	1.00	3.13	3.13
7	5.89	10	1.00	2.66	2.66
8	7.54	10	1.00	0.26	0.26
9	7.54	10	1.00	0.26	0.26

The maximum lengths and strains that occurred in each truss type are shown in Table VI.

TABLE VI
MAXIMUM STRAIN IN EACH TRUSS TYPE

Type	L_0 (m)	Maximum Length (m)	Max. Strain (%)
1	7.65	8.30	8.42
2	3.42	3.57	4.56
3	2.00	2.44	21.88
4	5.54	6.84	23.59
5	7.91	10.16	28.50
6	3.96	5.41	36.76
7	5.89	7.68	30.47
8	7.54	7.73	2.61
9	7.54	7.73	2.61

VI. CONCLUSIONS

A. *Achievements*

During this project a central difference scheme for dynamic analysis of a truss structure was produced and validated. A 3D deployable model was successfully programmed, and the central difference scheme applied. The 3D model deployed correctly within a reasonable time, given the parameters.

B. *Discussion of Results*

The elastic deployment analysis gave a minimum deployment time of 85.01 seconds. This would be an acceptable deployment time in space applications as most antennas are intended for long-term use and can afford several minutes for deployment, unless the antenna is to be used regarding communications for immediate orbit correction of the satellite. However, the deployment time is not an accurate approximation as the material data used was not realistic.

The maximum stresses occurred at the beginning of the deployment, as the structure is almost stress-free at full deployment. The maximum stress was 33.26 Pa.

This value is also not accurate as this analysis also did not take into account the mass and damping effects of the reflector surface and additional antenna components during deployment.

For the second analysis with an applied force of 0.03 N, the time to full deployment was 36.58 seconds. This is less than half the deployment time of the elastic deployment and would be more suitable for applications where the antenna must be deployed quickly for immediate use.

It is not useful at this stage to vary the applied force to reduce maximum stresses as the maximum stress occurs in the undeployed state and is not caused by the applied force during deployment. The applied force may have an effect on the maximum stresses experienced by the structure when realistic material data and the effects of the reflector surface are taken into account. A cable-net support for the reflector surface generally begins to affect the forces on the truss structure at around 90 % of deployment time [19].

The elastic deployment method may require some energy input to release the constraint mechanism and allow free deployment, though this is likely to require less power than the applied force deployment. This makes the elastic deployment method more suitable for situations where power sources are limited and long-term mission requirements allow a longer deployment time.

To conclude, both deployment systems have merits and could be useful for space applications, however deployment with an applied force reduces deployment significantly and would be more suitable for many applications.

C. *Future Work*

During this project, multiple areas could have been further developed but were not due to time and software constraints. Consequently, there are some areas which could be further investigated in the future.

In-depth analysis on the number of diagonal trusses necessary for deployment should be investigated in the future, along with optimisation of the number and type of diagonal members for strength, stiffness and mass.

Further exploration into material selections for the structure should also be carried out. The effects of the reflector surface of the antenna should be investigated

regarding mass and damping, along with the effects of other necessary equipment and components of the antenna that will be attached to the structure upon deployment.

Other work that could be explored includes optimising the hinge design for deployment, or using a click-joint hinge to eliminate oscillation of the structure and decrease deployment time. This type of joint in conjunction with the applied force deployment method could be used on permanent structures to massively reduce deployment time for applications where immediate use of the antenna is necessary. Click-joint hinges would also allow the use of tensioned cable-net as a reflector support.

Further comparison to non-ring deployable structures such as the hexagonal, triangular and square grid structures investigated by Chu et al [20], the cone structure investigated by Scialino et al [21], and the multiple structures presented by You et al [10,22] would be useful to determine the optimal deployable design to minimise mass and volume with sufficient stiffness.

Another deployment mechanism for potential future investigation is the slider-crank mechanism proposed by Li et al applied to a double-ring structure [2].

VII. Acknowledgment

I would like to thank my supervisor Professor Wulf Dettmer of Swansea University for his help and support.

VIII. References

[1] Qi X, Huang H, Li B, Deng Z. A large ring deployable mechanism for space satellite antenna. Aerospace Science and Technology [Internet]. 2016 [cited 2018 Oct 21];58:498–510. Available from: doi: 10.1016/j.ast.2016.09.014

[2] Li B, Qi X, Huang H, Xu W. Modeling and analysis of deployment dynamics for a novel ring mechanism. Acta Astronautica [Internet]. 2016 [cited 2018 Oct 22];120:59–74. Available from: doi: 10.1016/j.actaastro.2015.11.023

[3] Morterolle S, Maurin B, Dube J-F, Averseng J, Quirant J. Modal behavior of a new large reflector conceptual design. Aerospace Science and Technology [Internet]. 2015 [Cited 2018 Oct 31];42:74–9. Available from: doi: 10.1016/j.ast.2015.01.002

[4] Rey JJ, Wirth A, Jankevics A, Landers F, Rohweller D, Chen C B, et al. A deployable, annular, 30m telescope, space-based observatory; In: Space Telescopes and Instrumentation 2014: Optical, Infrared, and Millimeter Wave [Internet]. 2014 June 22-27; Montréal, Quebec, Canada. International Society for Optics and Photonics; 2014 [cited 2018 Dec 10]. p. 914318. Available from: doi: 10.1117/12.2057182

[5] Dai L, Guan F, Guest JK. Structural optimization and model fabrication of a double-ring deployable antenna truss. Acta Astronautica. 2014;94(2):843–51.

[6] MATLAB. Natick, Massachusetts, United States: The Mathworks, Inc.;2018.

[7] Davis GL, Tanimoto RL. Mechanical Development of Antenna Systems. In: Imbriale WA, editor. Spaceborne Antennas for Planetary Exploration [Internet]. Hoboken, NJ, USA: John Wiley & Sons, Inc.; 2006 [cited 2019 May 3]. p. 425–54. Available from: doi: 10.1002/0470052783.ch8

[8] Xu Y, Guan F, Xu X, Wang H, Zheng Y. Development of a Novel Double-Ring Deployable Mesh Antenna. International Journal of Antennas and Propagation [Internet]. 2012 [cited 2018 Oct 22]; 2012: Article ID 375463 [10 p.] Available from: doi: 10.1155/2012/375463

[9] Guan F, Dai L, Xia M. Pretension optimization and verification test of double-ring deployable cable net antenna based on improved PSO. Aerospace Science and Technology [Internet]. 2014 [Cited 2018 Oct 22];32(1):19–25. Available from: doi: 10.1016/j.ast.2013.11.008

[10] You Z, Pellegrino S. Cable-Stiffened Pantographic Deployable Structures Part 2: Mesh Reflector. AIAA Journal [Internet]. 1997 [Cited 2018 Nov 21];35(8):1348–55. Available from: doi: 10.2514/2.243

[11] Santiago-Prowald J, Baier H. Advances in deployable structures and surfaces for large apertures in space. CEAS Space Journal [Internet]. 2013 [Cited 2018 Nov 21];5(3-4):89–115. Available from: doi: 10.1007/s12567-013-0048-3

[12] Tibert G. Deployable Tensegrity Structures for Space Applications [PhD thesis on the Internet]. Stockholm: KTH Royal Institute of Technology; 2002 [Cited 2019 Mar 19]. Available from: https://www.researchgate.net/publication/244457217_Deployable_Tensegrity_Structures_for_Space_Applications

[13] Xu Y, Guan F, Chen J, Zheng Y. Structural design and static analysis of a double-ring deployable truss for mesh antennas. Acta Astronautica. 2012;81(2):545–54.

[14] Zhang Y, Ru W, Yang G, Li N. Deployment analysis considering the cable-net tension effect for deployable antennas. Aerospace Science and Technology [Internet]. 2016 [Cited 2018 Oct 21];48:193–202. Available from: doi: 10.1016/j.ast.2015.11.012

[15] Soares D, Großeholz G. Nonlinear structural dynamic analysis by a stabilized central difference method. Engineering Structures [Internet]. 2018 [Cited 2019 Mar 19];173:383–92. Available from: doi: 10.1016/j.engstruct.2018.06.115

[16] Yang B. Stress, Strain, and Structural Dynamics. [place unknown]: Elsevier; 2005.

[17] Khodaparast, H. H. (2018). Chapter 1: Vibration of Single Degree of Freedom Systems [Lecture notes]. Retrieved from https://blackboard.swan.ac.uk/bbcswebdav/pid-2448079-dt-content-rid-2594613_2/courses/1718_EG-260/Chapter1%281%29.pdf

[18] Cammarata A, Sinatra R, Rigato R, Maddio PD. Tie-System Calibration for the Experimental Setup of Large Deployable Reflectors. Machines [Internet]. 2019 [Cited 2019 May 3];7(2):23. Availale from: doi: 10.3390/machines7020023

[19] Zhang Y, Ru W, Yang G, Li N. Deployment analysis considering the cable-net tension effect for deployable antennas. Aerospace Science and Technology [Internet]. 2016 [Cited 2018 Oct 21];48:193–202. Available from: doi: 10.1016/j.actaastro.2016.11.038

[20] Chu Z, Deng Z, Qi X, Li B. Modeling and analysis of a large deployable antenna structure. Acta Astronautica [Internet]. 2014 [Cited 2018 Oct 31];95:51–60. Available from: doi: 10.1016/j.actaastro.2013.10.015

[21] Scialino L, Ihle A, Migliorelli M, Gatti N, Datashvili L, van ‘t Klooster K, et al. Large deployable reflectors for telecom and earth observation applications. CEAS Space Journal [Internet]. 2013 [Cited Mar 15];5(3–4):125–46. Available from: doi: 10.1007/s12567-013-0044-7

[22] You Z, Pellegrino S. Foldable bar structures. International Journal of Solids and Structures [Internet]. 1997 [Cited 2018 Nov 18];34(15):1825–47. Available from: doi: 10.1016/S0020-7683(96)00125-4